國立台灣大學理學院物理學研究所

碩士論文

Graduate Institute of Physics

College of Science

National Taiwan University

Master Thesis

微波加熱過程中的極化電荷屏蔽效應探討

Effects of Polarization-Charge Shielding in Microwave

Heating

林明勳

Ming-Syun Lin

指導教授：朱國瑞 教授

Advisor：Kwo-Ray Chu, Ph.D.

中華民國 104 年 7 月

July 2015

謝辭
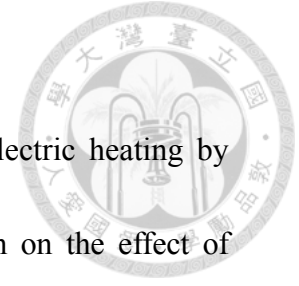
中文摘要

　　為了探討正處於興新領域的微波加熱介電材質，其基本物理問題，我們提出極化電荷造成的屏蔽效應理論，以及此效應在微波加熱的實驗觀察。把非球型的樣品放入微波暗室，並用均勻的行進波照射。由於極化電荷造成的屏蔽效應，樣品的加熱速率，取決於樣品的形狀與其相對外加電場的方向，而這可能就是造成溫差的主要成因。這是此意義重大的效應，首次被完整研究。

關鍵字：微波加熱，極化電荷屏蔽效應，微波暗室

英文摘要 Abstract

To address a basic physics issue in the growing field of dielectric heating by microwaves，we present the theory and experimental observation on the effect of polarization-charge shielding. Non-spherical samples are irradiated by a uniform traveling wave in an anechoic chamber. The polarization-charge shielded heating rate is shown to be highly dependent on the sample's shape and orientation relative to the wave electric field，which may become a major cause for an excessive temperature spread. This is a significant effect studied comprehensively for the first time，along with a demonstrated remedy.

Key words:　microwave heating，polarization charge shielding，anechoic chamber.

目錄

圖表錄

Chapter 1   Introduction

Radio frequency (RF) and microwaves penetrate much deeper into dielectric materials than the infrared radiation. Hence，dielectric heating by RF and microwaves allows far more rapid energy deposition to the bulk of the object than in a conventional furnace. This is an environmentally friendly method widely employed for scientific research and industrial applications. Examples include food processing [1], wood drying [2]，ceramic sintering [3, 4], medical treatment [5]，environmental engineering [6]，and insect control [7-8]. This is also a method still far from a mature stage. Current techniques need to be refined for more demanding applications，while new techniques，such as localized microwave heating [9]，are being developed for novel applications. On the other hand, microwave-assisted synthesis has become a burgeoning field of research in organic chemistry [10]，polymer science [11]，and drug discovery [12] only in the last decade.

The growing trend in sophisticated applications necessitates a deeper understanding of the physics issues concerning dielectric heating. As a specific example，for the protection of the ozone layer, the Montreal Protocol has stipulated a gradual phase-out of some of the most effective pesticides (such as methyl bromide). This has motivated active research on RF/microwave insect control，where the primary challenge has been to achieve a high degree of heating uniformity to avoid

damage to the host medium.

The RF region ranges from 3 kHz to 300 MHz and the microwave region from 300 MHz to 300 GHz. A frequency in the industrial，scientific，and medical (ISM) bands，notably 2.45 GHz，is often the choice for heating applications. The basic theory for dielectric heating applies to all bands. For practically all applications，uniform heating is highly desirable and，in many cases，of critical importance. Non-uniform heating can result in under-heated cold spots and thermal runaway due to accelerated heating at a hot spot，in addition to the difficulty of data analysis.

There are well-recognized reasons for non-uniform energy deposition，such as spatial field variations，shallow penetration depths，and inhomogeneous/anisotropic samples [2]. Somewhat less obvious is the shielding of the incident wave electric field by polarization charges induced on the sample. Exposed to an electromagnetic wave，a dielectric object's interior electric field can be shielded to a much smaller value than that of the surrounding wave. As a result，the heating rate is much reduced. Such effects have often been overlooked in the dielectric heating literature. In some cases，the well-known field reduction factor for a spherical object [Eq. (2) below] has been used to account for the polarization charge shielding (see，for example，[4] and [7]). As discussed later，a single reduction factor will be much too simplified to model the heating process of non-spherical objects，especially those with a relatively large

dielectric constant. To our knowledge，here has been no focused study on this crucial

effect although it is inherent in most experiments and simulations.
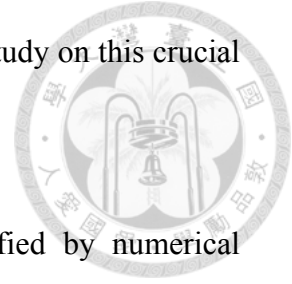
In the current study，it is shown in experiments and verified by numerical

simulations that such an effect can cause an excessively high temperature spread for

non-spherical objects. The study concludes with the demonstration of an effective

remedy to this deleterious effect.

Chapter 2   Theory of dielectric heating
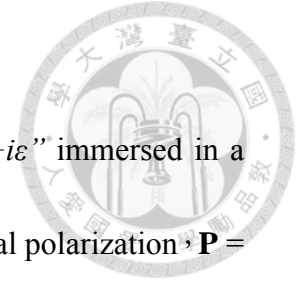
Consider a dielectric medium of complex permittivity $\varepsilon = \varepsilon'+i\varepsilon''$ immersed in a uniform AC electric field $\mathbf{E} = \mathbf{E}_d e^{-i\omega t}$. Time variation of the electrical polarization, $\mathbf{P} = (\varepsilon-\varepsilon_0)\mathbf{E}_d e^{-i\omega t}$, results in a polarization current density $\mathbf{J} = -i\omega(\varepsilon-\varepsilon_0)\mathbf{E}_d e^{-i\omega t}$, where ε_0 is the permittivity of free space. Thus, the power deposited into a unit volume can be written

$$P_d = \tfrac{1}{2}\text{Re}[\mathbf{J}\cdot\mathbf{E}*]=\tfrac{1}{2}\varepsilon''\omega|E_d|^2 , \qquad (1)$$

which is the commonly used expression for dielectric heating (see, for example, [1]-[4] and [8]).

2.1 Polarization-charge shielding of spherical objects

In Eq. (1), if $\varepsilon \gg \varepsilon_0$, the induced polarization charges on the sphere play an important role in shaping E_d. Consider the simple case of a uniform sphere immersed in a plane wave with an amplitude E_0 and a wavelength much greater than the radius of the sphere. The electric field (E_d) inside the dielectric sphere happens to be uniform, given by [13]

$$E_d = \frac{3\varepsilon_0}{\varepsilon + 2\varepsilon_0} E_0 \tag{2}$$

Substituting Eq. (2) into Eq. (1), we obtain

$$P_d = \frac{1}{2} \left[\frac{9\varepsilon_0^2}{\varepsilon'^2 + \varepsilon''^2 + 4\varepsilon_0\varepsilon' + 4\varepsilon_0^2} \right] \varepsilon'' \omega |E_0|^2 \tag{3}$$

Comparing Eqs. (1) and (3), the expression in the brackets in Eq. (3) gives the reduction factor in power absorption due to the polarization-charge shielding. As an example, the rubber wood has a moisture-dependent dielectric constant ($\varepsilon'/\varepsilon_0$) ranging from 2 to 35 at frequencies between 1 and 17 GHz [14]. Neglecting the much smaller loss factor ($\varepsilon''/\varepsilon_0$), Eq. (3) gives a power reduction factor between 0.75 and 0.0066 for the rubber wood. This illustrates a very significant shielding effect for high-permittivity objects commonly used in dielectric heating.

2.2 Polarization-charge shielding of non-spherical objects

Furthermore，as will be shown，the induced polarization-charge distribution and

hence its shielding effects are highly dependent on the object's (non-spherical) shape

as well as its orientation relative to the electric field. Given the same object，the power

reduction factor can easily vary by more than one order of magnitude. This provides a

means for a direct experimental observation of the orientation- and shape-dependent

power reduction factor.

Chapter 3   Features of the experimental setup

The microwave applicator used for the present experiment   [Fig. 1(b)]，a

60 cm x 60 cm x 60 cm anechoic chamber [15], is radically different from the

commonly-used，resonator-type microwave oven. It features traveling-wave radiation

emitted from a lab-made，24-GHz，kW-level，extended interaction oscillator (EIO)

[16]. As shown in Fig. 1(a)，the EIO output wave first passes through a calibrated

diagnostic circuit for power and frequency measurements before entering a

polarization converter [17，18]，in which it is converted into a circularly-polarized

wave and then input into a conical horn antenna, from which it is radiated into the

chamber [Fig. 1(b)]. The wave can also bypass the polarization converter to enter the

horn antenna in linearly-polarized state. A height-adjustable sample holder receives

the radiation along the axis of the antenna. An IR camera is attached to a rotatable

mount，which can slide horizontally on the top wall or up and down on a side wall. It

records real-time，digital images of the heated sample surface.
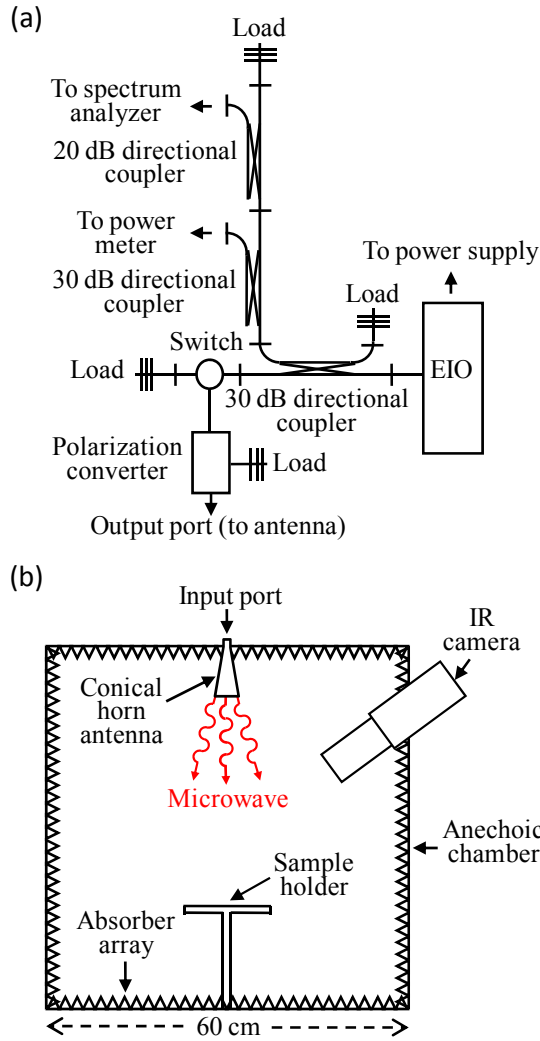
Fig. 1. Schematics of the microwave applicator system. (a) The radiation source (a 24-GHz EIO)，diagnostic circuit, and polarization converter. (b) The anechoic chamber，conical horn antenna，and IR camera.

Figure 2 shows a 1 mm x 1 mm x 8 mm，wood-stick sample lying on the sample holder (the *x-y* plane). The sample's orientation angle (θ) with respect to the *y*-axis can be adjusted from 0° to 180° by a rotation about the *z*-axis. Placed at a distance of 18 cm away from the horn opening, the sample sees essentially a uniform plane wave.

The simulated radiation pattern [15] predicts a maximum intensity variation of only

1% over the sample area. By comparison，if the same sample were placed in the 24

GHz standing wave of a microwave resonator，it would see an 100% intensity

variation. With non-reflecting walls on all sides，this is practically the only radiation

on the sample. Also，we have chosen a sample thickness (1 mm) much thinner than

one wavelength (12.5 mm) so that the polarization-charge shielding is not

complicated by spatial field variations within the sample. This simple experimental

environment allows highly reproducible data acquisition and *in situ* diagnostics，as

well as a reliable numerical verification of the observed data.
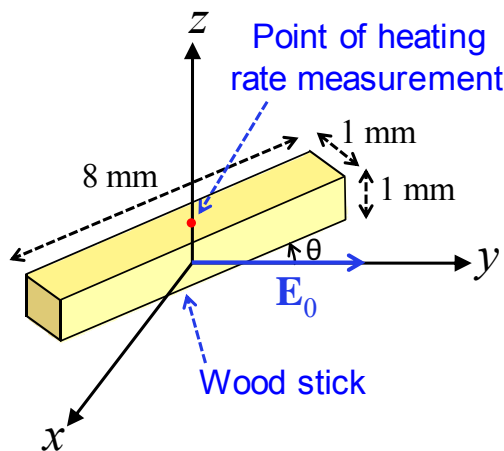
Fig. 2. Dimensions of the wood-stick sample lying on the *x-y* plane at an

adjustable orientation angle (θ) with respect to the *y*-axis. The traveling wave

is directed downward toward the sample. For a linearly polarized wave，its

electric field ($\mathbf{E}_0$) is in the *y*-direction.

Chapter 4　Experimental　observation　of Polarization - charge　shielding

During the microwave heating，the sample was exposed to the same intensity of $\sim 12.9.W/cm^2$ at different orientation angles (θ). The heating was stopped at a temperature (T) a few degrees above the room temperature so as to minimize the convection loss and least affect the sample's dielectric property. IR images of the heated wood stick by a linearly-polarized wave are shown in Fig. 3. The temperature rise profiles were measured *in situ* at the center of the sample's upper surface and digitally recorded.

(a) θ = 0 ° (b) θ = 90 °
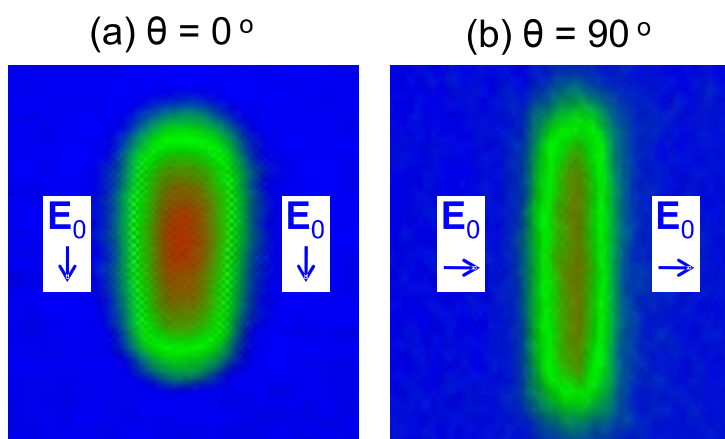
Fig. 3. IR images of the wood stick heated by a linearly-polarized wave shown in Fig. 2. The red color denotes a higher temperature. The center spot is ~6.81 times hotter at $\theta = 0^0$ than at $\theta = 90^0$ [see Fig. 4(a)].

Data points taken in the early stage of power application (negligible convection heat loss) give a constant heating rate (dT/dt), which is plotted as a function of θ in Fig. 4(a) for the linearly polarized incident wave with the electric field ($\mathbf{E}_0$) in the y-direction (Fig. 2). The polarization-charge shielding leads to a strong angular dependence of the heating rate，with a maximum at $\theta = 0^{\text{o}}$ and a minimum at $\theta = 90^{\text{o}}$. The maximum-to-minimum ratio is ~6.81 at the center spot，as shown in Fig. 4(a).
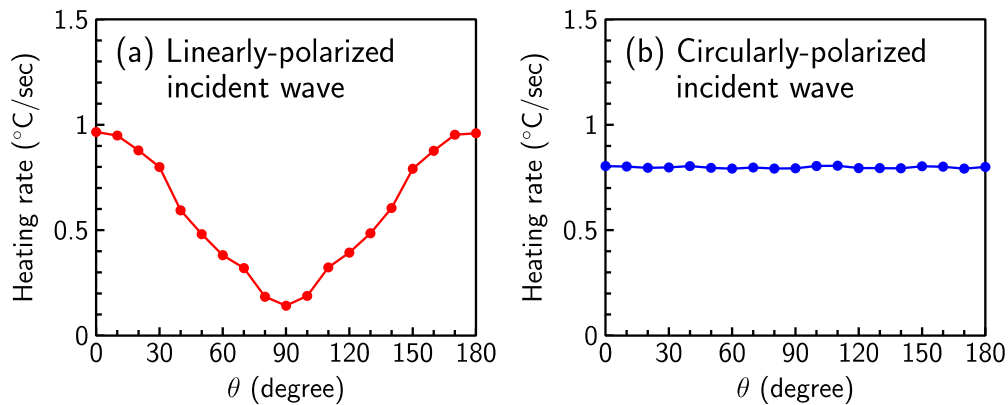
Fig. 4. Heating rate of the wood stick in Fig. 2 as a function of θ during the initial stage of power application. (a) By a linearly-polarized wave；(b) By a circularly-polarized wave.

Chapter 5   An effective remedy
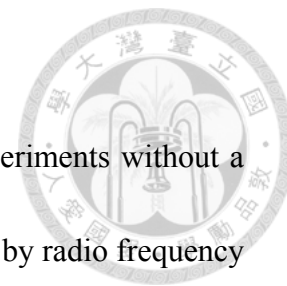
Effects of sample orientation have been observed in early experiments without a clear physical interpretation. For example，in walnut pests control by radio frequency heating [19]，the temperature increment for $\theta = 0^o$ oriented walnuts was 25% higher than that of the $\theta = 90^o$ oriented ones，which was remedied by a tumbling process.

Here，we consider an electronic remedy by applying a circularly polarized incident wave (emitted from the same antenna). The rapid rotation of the $\mathbf{E}_0$ vector is expected to result in a heating rate independent of θ. Indeed，as shown in Fig.4(b)，the heating rate at the center spot now varies by at most 0.9% in the range of $\theta = 0^o$-180°.

Chapter 6   Physical interpretation by

numerical   simulation

On the basis of the model shown in Fig.2 and using the HFSS code，we have

numerically evaluated the electromagnetic field profile for $\theta = 0^o$ and 90° under the

application of a fixed-power，24 GHz，linearly-polarized wave. The best fit to the

experimental data occurs at $\varepsilon/\varepsilon_0 = 4.7 + 0.12i$. At the center of the upper wood surface

($x = y = 0$，$z = 1$ mm)，this gives a heating rate 6.815 times higher at $\theta = 0^o$ than at θ

$= 90^o$，as is consistent with the measured value.   For the wood medium，we have

$\varepsilon' >> \varepsilon''$. Thus, the field profiles are more sensitive to ε' than to ε''. With $\varepsilon'/\varepsilon_0 = 4.4$

and 5.0，the maximum-to-minimum ratio becomes 6.0 and 7.8，respectively.

Figure 5 shows the simulated electric field strength (in color code) on the center

plane of the wood stick (the $z = 0.5$ mm plane in Fig. 2). By Gauss law，the presence

of polarization charges is evidenced by the sharp discontinuities of the overall electric

field strength. In the $\theta = 0^o$ case，the incident electric field ($\mathbf{E}_0$) is along the length of

the wood stick. The induced polarization charges essentially form two surface charge

layers of opposite signs at the two ends. However，these charges are too confined and

too far apart to significantly affect the electric field inside the sample. For the $\theta = 90^o$

case，$\mathbf{E}_0$ is perpendicular to two broad sides of the wood stick. In sharp contrast，there

is now an extended distribution of surface charges on the two side walls，again of

opposite signs but with a much narrower separation. This results in a substantial

cancellation of the incident electric field，and hence the much reduced heating rate.
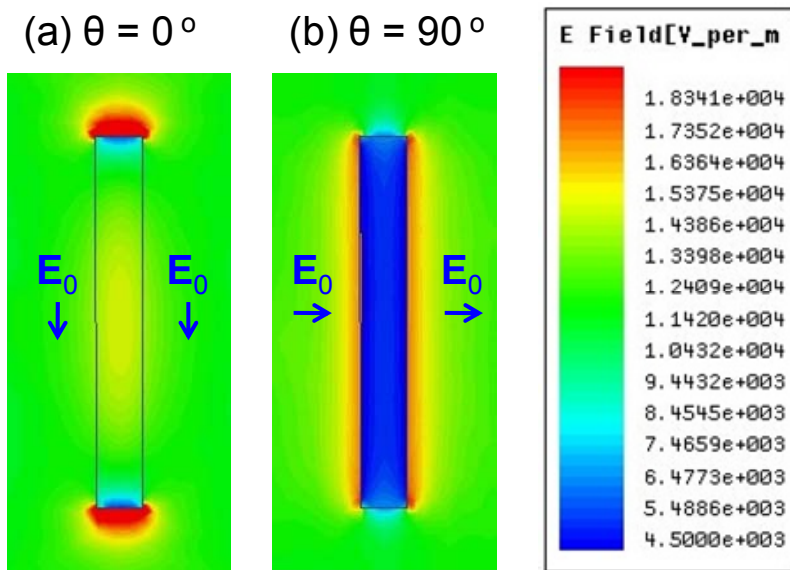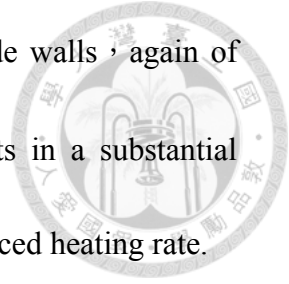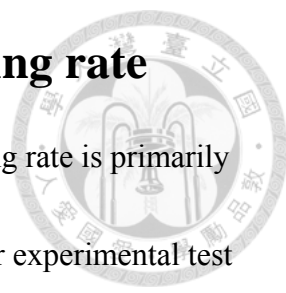
Fig. 5. Simulated electric field strength (shown in color code) on the center

plane of the wood stick (the $z = 0.5$ mm plane in Fig. 2) as it is heated by a

linearly-polarized wave (with **E** shown in Fig. 2). (a) $\theta = 0^0$; (b) $\theta = 90^0$.

Chapter 7 　 Shape dependence of the heating rate

According to Fig. 5，the sensitive angular dependence in heating rate is primarily due to the elongated shape of the sample. Figure 6 displays a similar experimental test for a less elongated sample，a rice grain approximately elliptical in shape，with maximum lengths of 5.0 mm，3.0 mm，and 1.9 mm in the x，y，and z directions，respectively. While the long wood stick sample represents a scaled-down model of，for example，13.6-MHZ wood drying [2]，the rice grain sample is a scaled-down model applicable to heating of small objects in the 2.45-GHz household microwave oven. The incident wave (linearly polarized) has resulted in a much small angular dependence of the heating rate，but still up to a factor of ~2 at the center point on the top surface [Fig. 6(a)]. A difference of such a magnitude has an important bearing on, for example, insect control of stored grains by RF and microwaves. As shown in Fig. 6(b)，angular dependence of the heating rate is again eliminated by the application of a circularly-polarized wave.

Chapter 8　Summary
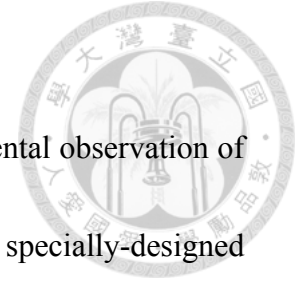
In summary，we have presented a direct and focused experimental observation of polarization-charge shielding effects in microwave heating. In a specially-designed microwave applicator，the heating rate of a long wood stick is found to differ by a factor up to 6.8，depending on its orientation relative to the wave field. For a less-elongated and elliptically-shaped rice grain，the orientation still causes a heating rate difference as high as 2.
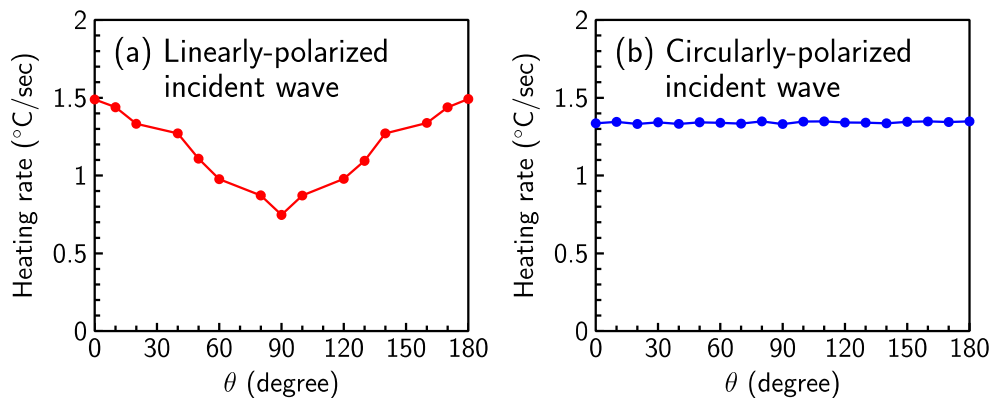
Fig. 6. Heating rate of a rice grain as a function of θ during the initial stage of power application. (a) By a linearly-polarized wave ; (b) By a circularly-polarized wave.

16

The results are physically interpreted by numerical simulations. Such effects are expected to significantly degrade the temperature uniformity of heated objects, especially those with a high dielectric constant. The study concludes with a demonstration that a circularly-polarized wave may eliminate this major cause of heating non-uniformity，although other (often less serious) causes still remain. A physical insight into these effects and the proposed remedy are expected to be of high reference value to a broad range of conventional and emerging fields involving microwave heating.
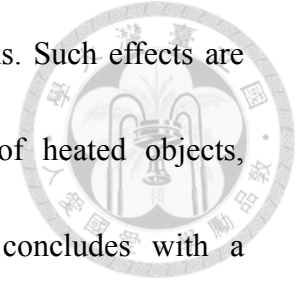
附錄 A　紅外線熱像儀（IR camera）

　　所有溫度在絕對零度（約-273℃）以上的物體，都會因自身的分子運動而產生紅外線輻射熱。　紅外線熱像儀能將這些輻射能量轉換為電訊號。接著用各種不同顏色來顯示出不同溫度的分佈，並以可視圖像顯示出來，如圖 A-1。
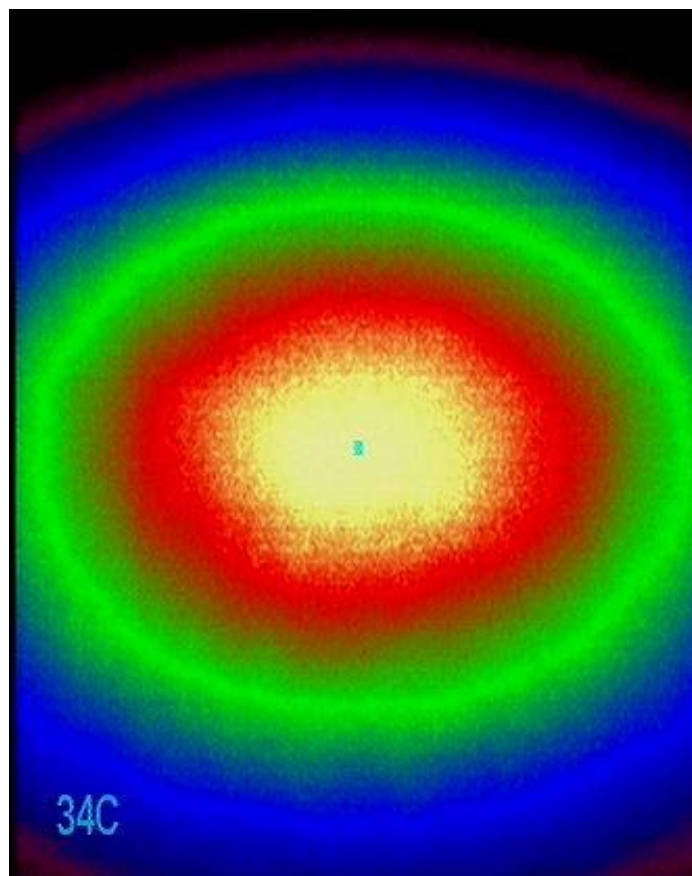
圖 A-1　一張紙在 24GHz 且電場圓極化的微波加熱溫度分佈圖。

白色溫度最高，黃色次之，愈往外圍溫度愈低，中心點溫度

顯示在左下角。

紅外線熱像儀可以從物體表面輻射，並推算出物體的表面溫度。根據

Stefan–Boltzmann's Law ： $J = \varepsilon \sigma T^4$

（ 黑體的表面每平方公尺、每秒鐘所產生的電磁輻射能量 ）

從上式可看出，當物體溫度高時，黑體輻射放射率 ε（emissivity）對物體輻射

通量 J 的影響會變大，從而影響紅外線熱像儀量得的溫度。所以在量測高溫物

體時，要先對黑體輻射放射率作校正。

圖 A-4 為 4 mm × 4 mm SiC 薄片，平放在電阻中心，並用一種良好的熱傳

導材料將兩者連接在一起。此舉能減少兩者接觸面的空隙，以確保電阻通電時，

電阻產生的熱能可以均勻傳遞給 SiC 薄片。實驗上的操作為：每次增加一點電

壓，使電阻緩慢升溫，並與 SiC 薄片達到熱平衡。接著利用熱電偶（Thermocouple）

與紅外線熱像儀同時測量 SiC 薄片的溫度，當調整熱像儀的放射率（emissivity）

為 80％時，就可發現熱電偶與熱像儀，兩者量到的溫度互相吻合。

圖 A-4 熱像儀放射率校正圖。熱電偶（Thermocouple）與紅外線熱像儀（IR

camera）同時測量 SiC 加熱溫度，藉此校正 SiC 黑體輻射放射率。

附錄 B　HFSS 模擬：24GHz 線極化微波加熱均勻度

(圓形號角天線，輸入功率 1 kW)

表 B-1：X 方向（ 偏振方向 ）加熱均勻度（uniformity）

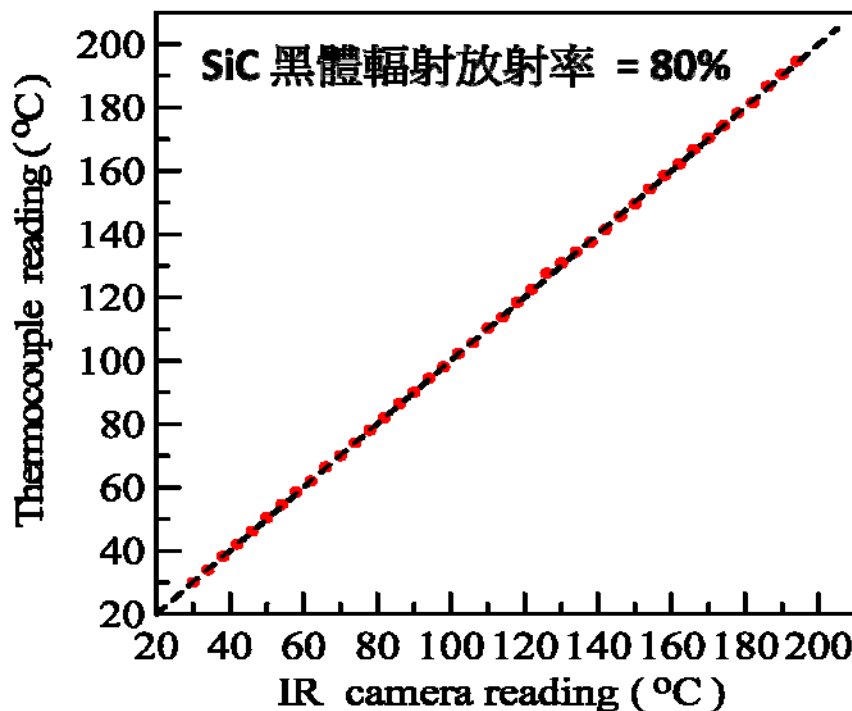| Distance (cm)	1	2	3	4	5	6	7	8
D = 1 cm	116.34%	114.30%	86.97%	83.85%	85.83%	88.36%	90.55%	92.28%
D = 2 cm	102.77%	108.65%	64.86%	54.20%	56.28%	61.80%	67.56%	72.64%
D = 4 cm	23.13%	19.68%	21.41%	21.49%	20.19%	21.07%	24.65%	29.99%
D = 6 cm	2.58%	4.21%	2.66%	5.16%	8.28%	9.70%	10.18%	11.11%
D = 8 cm	0.50%	1.52%	1.24%	0.84%	1.87%	3.87%	5.50%	6.32%
D = 10 cm	0.22%	0.57%	0.76%	0.61%	0.42%	0.90%	2.10%	3.41%
Distance (cm)	9	10	11	12	13	14	15	16
D = 1 cm	93.62%	94.66%	95.48%	96.13%	96.65%	97.08%	97.43%	97.73%
D = 2 cm	76.86%	80.30%	83.10%	85.38%	87.25%	88.80%	90.10%	91.19%
D = 4 cm	36.08%	42.21%	48.00%	53.28%	58.01%	62.19%	65.86%	69.09%
D = 6 cm	13.17%	16.37%	20.44%	25.01%	29.79%	34.56%	39.17%	43.53%
D = 8 cm	6.71%	7.27%	8.41%	10.27%	12.82%	15.91%	19.38%	23.07%
D = 10 cm	4.36%	4.84%	5.10%	5.43%	6.10%	7.22%	8.83%	10.90%
Distance (cm)	17	18	19	20	21	22	23	24
D = 1 cm	97.97%	98.18%	98.36%	98.51%	98.64%	98.76%	98.86%	98.95%
D = 2 cm	92.11%	92.90%	93.58%	94.16%	94.68%	95.12%	95.52%	95.87%
D = 4 cm	71.93%	74.43%	76.63%	78.57%	80.30%	81.83%	83.21%	84.43%
D = 6 cm	47.61%	51.39%	54.86%	58.04%	60.95%	63.61%	66.04%	68.26%
D = 8 cm	26.86%	30.65%	34.36%	37.95%	41.38%	44.64%	47.71%	50.61%
D = 10 cm	13.35%	16.08%	19.01%	22.07%	25.18%	28.30%	31.38%	34.39%
Distance (cm)	25	26	27	28	29	30	31	32
D = 1 cm	99.03%	99.10%	99.17%	99.22%	99.28%	99.32%	99.36%	99.40%
D = 2 cm	96.18%	96.46%	96.70%	96.93%	97.13%	97.31%	97.48%	97.63%
D = 4 cm	85.53%	86.53%	87.42%	88.24%	88.97%	89.65%	90.26%	90.82%
D = 6 cm	70.29%	72.14%	73.84%	75.40%	76.84%	78.15%	79.37%	80.49%
D = 8 cm	53.32%	55.86%	58.23%	60.44%	62.51%	64.43%	66.23%	67.91%
D = 10 cm	37.30%	40.12%	42.82%	45.40%	47.86%	50.19%	52.41%	54.51%
Distance (cm)	33	34	35	36	37	38	39	40
D = 1 cm	99.44%	99.47%	99.50%	99.53%	99.55%	99.57%	99.60%	99.61%
D = 2 cm	97.77%	97.89%	98.01%	98.11%	98.21%	98.30%	98.39%	98.47%
D = 4 cm	91.34%	91.81%	92.25%	92.65%	93.03%	93.37%	93.69%	93.99%
D = 6 cm	81.52%	82.48%	83.37%	84.20%	84.96%	85.68%	86.34%	86.97%
D = 8 cm	69.48%	70.94%	72.31%	73.60%	74.80%	75.92%	76.98%	77.97%
D = 10 cm	56.50%	58.38%	60.16%	61.85%	63.44%	64.95%	66.37%	67.72%
Distance (cm)	41	42	43	44	45	46	47	48
D = 1 cm	99.63%	99.65%	99.67%	99.68%	99.69%	99.71%	99.72%	99.73%
D = 2 cm	98.54%	98.61%	98.67%	98.73%	98.78%	98.84%	98.88%	98.93%
D = 4 cm	94.27%	94.53%	94.77%	95.00%	95.21%	95.41%	95.60%	95.78%
D = 6 cm	87.55%	88.09%	88.60%	89.08%	89.53%	89.96%	90.35%	90.73%
D = 8 cm	78.90%	79.78%	80.61%	81.39%	82.12%	82.82%	83.47%	84.09%
D = 10 cm	68.99%	70.20%	71.35%	72.43%	73.46%	74.43%	75.36%	76.24%
Distance (cm)	49	50						
D = 1 cm	99.74%	99.75%						
D = 2 cm	98.97%	99.01%						
D = 4 cm	95.94%	96.10%						
D = 6 cm	91.09%	91.42%						
D = 8 cm	84.68%	85.24%						
D = 10 cm	77.08%	77.87%						

表 B-2： Y 方向加熱均勻度（uniformity）

Distance（cm）	1	2	3	4	5	6	7	8
D = 1cm	98.37%	84.22%	78.31%	82.91%	87.29%	90.41%	92.56%	94.09%
D = 2 cm	64.26%	54.33%	41.81%	48.74%	58.46%	66.80%	73.29%	78.23%
D = 4 cm	3.25%	8.22%	9.05%	10.10%	14.29%	21.31%	29.58%	37.85%
D = 6 cm	0.13%	0.52%	1.41%	2.52%	3.39%	4.84%	7.74%	12.14%
D = 8 cm	0.02%	0.06%	0.18%	0.57%	1.14%	1.62%	2.18%	3.30%
D = 10 cm	0.01%	0.02%	0.04%	0.12%	0.35%	0.68%	0.98%	1.26%
Distance（cm）	9	10	11	12	13	14	15	16
D = 1cm	95.19%	96.02%	96.66%	97.15%	97.54%	97.86%	98.12%	98.33%
D = 2 cm	82.01%	84.94%	87.23%	89.05%	90.51%	91.71%	92.70%	93.52%
D = 4 cm	45.45%	52.17%	57.97%	62.94%	67.18%	70.80%	73.89%	76.55%
D = 6 cm	17.60%	23.59%	29.66%	35.54%	41.06%	46.14%	50.77%	54.94%
D = 8 cm	5.30%	8.24%	11.97%	16.25%	20.83%	25.52%	30.16%	34.65%
D = 10 cm	1.72%	2.62%	4.11%	6.24%	8.94%	12.10%	15.59%	19.28%
Distance（cm）	17	18	19	20	21	22	23	24
D = 1cm	98.51%	98.67%	98.80%	98.91%	99.01%	99.09%	99.16%	99.23%
D = 2 cm	94.21%	94.80%	95.30%	95.74%	96.12%	96.45%	96.74%	96.99%
D = 4 cm	78.85%	80.84%	82.57%	84.08%	85.42%	86.59%	87.64%	88.57%
D = 6 cm	58.69%	62.06%	65.08%	67.78%	70.22%	72.41%	74.38%	76.16%
D = 8 cm	38.92%	42.95%	46.71%	50.20%	53.43%	56.41%	59.16%	61.69%
D = 10 cm	23.06%	26.85%	30.57%	34.19%	37.66%	40.98%	44.13%	47.10%
Distance（cm）	25	26	27	28	29	30	31	32
D = 1cm	99.29%	99.34%	99.39%	99.43%	99.46%	99.50%	99.53%	99.56%
D = 2 cm	97.22%	97.42%	97.60%	97.76%	97.91%	98.04%	98.16%	98.27%
D = 4 cm	89.40%	90.14%	90.81%	91.41%	91.96%	92.46%	92.91%	93.33%
D = 6 cm	77.77%	79.23%	80.56%	81.76%	82.87%	83.88%	84.81%	85.66%
D = 8 cm	64.02%	66.17%	68.15%	69.98%	71.66%	73.22%	74.66%	75.99%
D = 10 cm	49.90%	52.53%	54.99%	57.31%	59.47%	61.50%	63.39%	65.17%
Distance（cm）	33	34	35	36	37	38	39	40
D = 1cm	99.58%	99.61%	99.63%	99.65%	99.66%	99.68%	99.70%	99.71%
D = 2 cm	98.37%	98.46%	98.55%	98.63%	98.70%	98.76%	98.82%	98.88%
D = 4 cm	93.71%	94.05%	94.37%	94.67%	94.94%	95.19%	95.43%	95.64%
D = 6 cm	86.44%	87.16%	87.83%	88.45%	89.02%	89.55%	90.05%	90.51%
D = 8 cm	77.23%	78.38%	79.45%	80.44%	81.37%	82.24%	83.04%	83.80%
D = 10 cm	66.83%	68.39%	69.84%	71.21%	72.50%	73.70%	74.84%	75.90%
Distance（cm）	41	42	43	44	45	46	47	48
D = 1cm	99.72%	99.74%	99.75%	99.76%	99.77%	99.78%	99.79%	99.80%
D = 2 cm	98.93%	98.98%	99.03%	99.07%	99.11%	99.15%	99.18%	99.21%
D = 4 cm	95.85%	96.04%	96.21%	96.38%	96.53%	96.67%	96.81%	96.94%
D = 6 cm	90.94%	91.34%	91.72%	92.07%	92.40%	92.71%	93.00%	93.28%
D = 8 cm	84.51%	85.17%	85.80%	86.39%	86.94%	87.46%	87.95%	88.41%
D = 10 cm	76.91%	77.85%	78.75%	79.59%	80.38%	81.13%	81.84%	82.52%
Distance（cm）	49	50						
D = 1cm	99.80%	99.81%						
D = 2 cm	99.25%	99.27%						
D = 4 cm	97.06%	97.17%						
D = 6 cm	93.54%	93.78%						
D = 8 cm	88.85%	89.26%						
D = 10 cm	83.15%	83.76%						

REFERENCES

[1] P. Piyasena, C. Dussault, T. Koutchma, H. S. Ramaswamy, and G. B. Awuah, Crit.

Rev. Food Sci. Nutr. **43**, 587 (2003).

[2] H. Resch, Maderas Cinecia y Tecnologia **8**, 67 (2006).

[3] M. Oghbaei and O. Mirzaee, J. Alloys and Compounds **494**, 175 (2010).

[4] K. I. Rybakov, E. A. Olevsky, and E.V. Krikun, J. Am. Ceram. Soc., **96** 1003

(2013).

[5] A. Rosen, M. A. Stuchly, and A. V. Vorst, IEEE Trans. Microwave Theory

Techniques **50**, 963 (2002).

[6] D. A. Jones, T. P. Lelyveld, S. D. Mavrofidis, S. W. Kingman, and N. J. Miles,

Resources, Conservation and Recycling **34**, 75 (2002).

[7] S. O. Nelson, Trans. ASAE **39**(4), 1475 (1996).

[8] S. Wang, J. Tang, J. A. Johnson, R. P. Cavalieri, J. Stored Products Research **55**,

15 (2013).

[9] E. Jerby, Y. Meir, A. Salzberg, E. Aharoni, A. Levy, J. P. Torralba, B. Cavallini,

Additive Manufacturing **6**, 53 (2015).

[10] C. O. Kappe, A. Stadler, and D. Dallinger, *Microwaves in Organic and

Medicinal Chemistry* (Wiley-VCH, Weinheim, Germany, 2012).

[11] A. Mishra, T. Vats, and J. Clark, *Microwave-Assisted Polymerization* (Royal

Society of Chemistry, Oxfordshire, UK, 2015).

[12] *Microwaves in Drug Discovery and Development: Recent Advances*, edited by J. Spencer and M. C, Bagley (Future Science, London, UK, 2014).

[13] J. D. Jackson, *Classical Electrodynamics*, third edition (John Wiley, New York, 1998), Eq. (4.55).

[14] M. F. Kabir, K. B. Khalid, W. M. Daud, and S. H. A. Aziz, Wood and Fiber Sci. **29**, 319 (1997).

[15] W. Y. Chiang, M. H. Wu, K. L. Wu, M. H. Lin, H. H. Teng, Y. F. Tsai, C. C. Ko, E. C. Yang, J. A. Jiang, L. R. Barnett, and K. R. Chu, Rev. Sci. Instru. **85**, 084703 (2014).

[16] L. Chen, H. Guo, H.Y. Chen, M. H.Tsao, T. T. Yang, Y. C. Tsai, and K. R. Chu, IEEE Trans. Plasma Science **28**, 626 (2000).

[17] L. R. Barnett, L. H. Chang, H. Y. Chen, K. R. Chu, W. K. Lau and C. C. Tu, Phys. Rev. Lett. **63**, 1062 (1989).

[18] T. H. Chang, L. R. Barnett, K. R. Chu, F. Tai, and C. L. Hsu, Rev. Sci. Instrum. **70**, 1530 (1999).

[19] S. Wang, J. Tang, T. Sun, E. J. Mitcham, T. Koral, S. L. Birla, J. Food Engin. **77**, 304 (2006).